

Reconfigurable synthesizer for quantum information processing of high-dimensional entangled photons

Ohad Lib, Kfir Sulimany and Yaron Bromberg*

Racah Institute of Physics, The Hebrew University of Jerusalem, Jerusalem, 91904 Israel

*To whom correspondence should be addressed; E-mail: Yaron.Bromberg@mail.huji.ac.il.

Abstract

High-dimensional entangled photons are a key resource for advanced quantum information processing. Efficient processing of high-dimensional entangled photons requires the ability to synthesize their state using general unitary transformations. The leading technology for processing photons in high-dimensions is integrated multiport interferometers. However, such devices are incompatible with free-space and fiber-based systems, and their architecture poses significant scaling challenges. Here we unlock these limitations by demonstrating a reconfigurable processor of entangled photons that is based on multi-plane light conversion (MPLC), a technology that was recently developed for multiplexing hundreds of spatial modes for classical free-space and fiber communication. To demonstrate the flexibility of MPLC, we perform four key tasks of quantum information processing using the same MPLC hardware: entanglement certification, tailored two-photon interference, arbitrary state transformations, and mode conversion. Based on the high degree of control we obtain, we expect MPLC will become a leading platform for future quantum technologies.

Photonic platforms are indispensable for both fundamental tests of quantum mechanics and quantum information processing [1]. A key ingredient in almost every quantum information processing protocol is a programmable synthesizer of quantum states [2, 3]. In particular, entanglement processing, distribution and certification are essential steps required in a wide range of applications such as device-independent quantum key distribution (QKD) [4–6], one-way quantum computation [7, 8] and for fundamental tests of quantum mechanics [9, 10]. Arbitrary random unitary transformations also offer an alternative route towards demonstrating quantum supremacy via boson sampling [11, 12]. To support such applications, ideal quantum processors should be reconfigurable, scalable and capable of performing arbitrary unitary transformations with high fidelities [2].

Over the past few years, reconfigurable multiport interferometers were developed for on-chip transformations of single and entangled photons [2,3,13–17]. To date, most demonstrations of $N \times N$ transformations for N modes relied on a mesh of $\sim N^2$ integrated Mach-Zehnder interferometers and phase shifters. The quadratic scaling with the number of interferometers makes the integrated approach sensitive to fabrication errors and interferometric noise. Moreover, integrated processors are incompatible with recent breakthroughs in increasing the capacity of classical and quantum channels by encoding high-dimensional bits of information in the transverse modes of photons [18–21]. Recently, a new approach compatible with high-dimensional encoding with transverse modes was proposed and demonstrated, using wavefront shaping and a multi-mode fiber as a reconfigurable multimode processor [22]. While being a promising direction for studying linear quantum networks, it has limited applicability for many quantum information processing tasks since it requires careful characterization of the complex transmission matrix of the multimode fiber, which limits the available optical bandwidth and temporal stability [22, 23].

In this work we implement a solution developed for multimode processing in classical optical communication, for high-dimensional entangled photons. The need to deploy efficient and compact multimode multiplexers for spatial division multiplexing, has led to the development of multi-plane light conversion (MPLC) technology. It is based on performing general and reconfigurable unitary transformations on spatial modes of classical light, using only a few optimized phase masks separated by free-space propagation [24, 25]. MPLC has several unique features which make it attractive to quantum information processing. It exhibits high phase stability due to its common path configuration, and it offers extremely wide-band operation [26, 27]. Most importantly, the number of phase masks required for obtaining a good approximation of arbitrary unitary transformations scales only linearly with the number of manipulated modes, making this approach potentially scalable [24, 25, 28]. Recently, an impressive line of works have demonstrated the use of MPLC for sorting over a thousand spatial modes with only 14 phase masks [29, 30] and to simultaneously control all degrees of freedom of classical light [31]. In the quantum regime, MPLCs were used for performing unitary gates on single photons in high-dimensions [32] and for studying two-photon interference of separable orbital angular momentum states [27]. Nevertheless, the full potential of MPLC as a tool for quantum information processing is yet to be fulfilled, as only a few specific transformations on separable input states have been considered, precluding crucial tasks for quantum information processing such as general transformations of entangled photons and high-dimensional entanglement certification [33].

We demonstrate the applicability of MPLC as a general and potentially scalable platform for quantum information processing of entangled photons. We perform four key tasks for quantum information processing: high-dimensional entanglement certification, tailored two-photon interference, arbitrary random transformations and spatial mode conversions for entanglement distribution. All tasks are performed by simply changing the reconfigurable phase patterns employed by the MPLC, without any changes in the hardware. To certify two- and three-dimensional entanglement and observe tailored two-photon interference, we program the MPLC

to switch between mutually unbiased bases (MUBs) [34]. To demonstrate the universality of MPLC processing we experimentally realize 400 Haar random unitary transformations with high statistical fidelity on four spatial modes [2, 3]. Finally, we demonstrate mode conversion of the original path-encoded state to a linearly polarized (LP) mode basis fits for entanglement distribution via a few-mode fiber link [35–38]. These results pave the way towards the implementation of MPLC as an important building block for high-dimension quantum information processing tasks such as entanglement certification, boson sampling, entanglement distribution and quantum key distribution.

Results

The concept of synthesizing the quantum state of entangled photons is depicted in fig. 1a. The two-photon entangled state is encoded using $2N$ spatial modes in the so called pixel basis [39,40]. The N upper (lower) modes are labeled as $|1\rangle_A, \dots, |N\rangle_A$ ($|1\rangle_B, \dots, |N\rangle_B$). The desired unitary operation is programmed onto the MPLC which transforms the input state accordingly, and the correlations between different output modes are then measured using single photon detectors.

Experimentally, we generate the spatially entangled input state via spontaneous parametric down conversion (SPDC) by pumping a nonlinear crystal with a pump laser beam (fig. 1b). The MPLC is located at the far-field of the crystal, thus, due to transverse momentum correlations in SPDC, the input quantum state is spatially entangled and is approximately given by $|\psi\rangle = \frac{1}{\sqrt{N}}(|1\rangle_A|1\rangle_B + \dots + |N\rangle_A|N\rangle_B)$. We experimentally implement a five-plane MPLC by successive reflections of the photons between a phase-only spatial light modulator (SLM) and a mirror. The algorithm for finding the required phase masks for a desired unitary transformation is based on the wavefront-matching algorithm [29] (see Methods). The output modes of the transformation can be chosen according to the specific application. In most of our experiments, Gaussian spots located in an equally spaced column are chosen in order to facilitate coupling to a fiber array. In this experiment however, we use two scanning single photon detectors to obtain the quantum correlations between all relevant modes. More details regarding the experimental setup are given in the supplementary information.

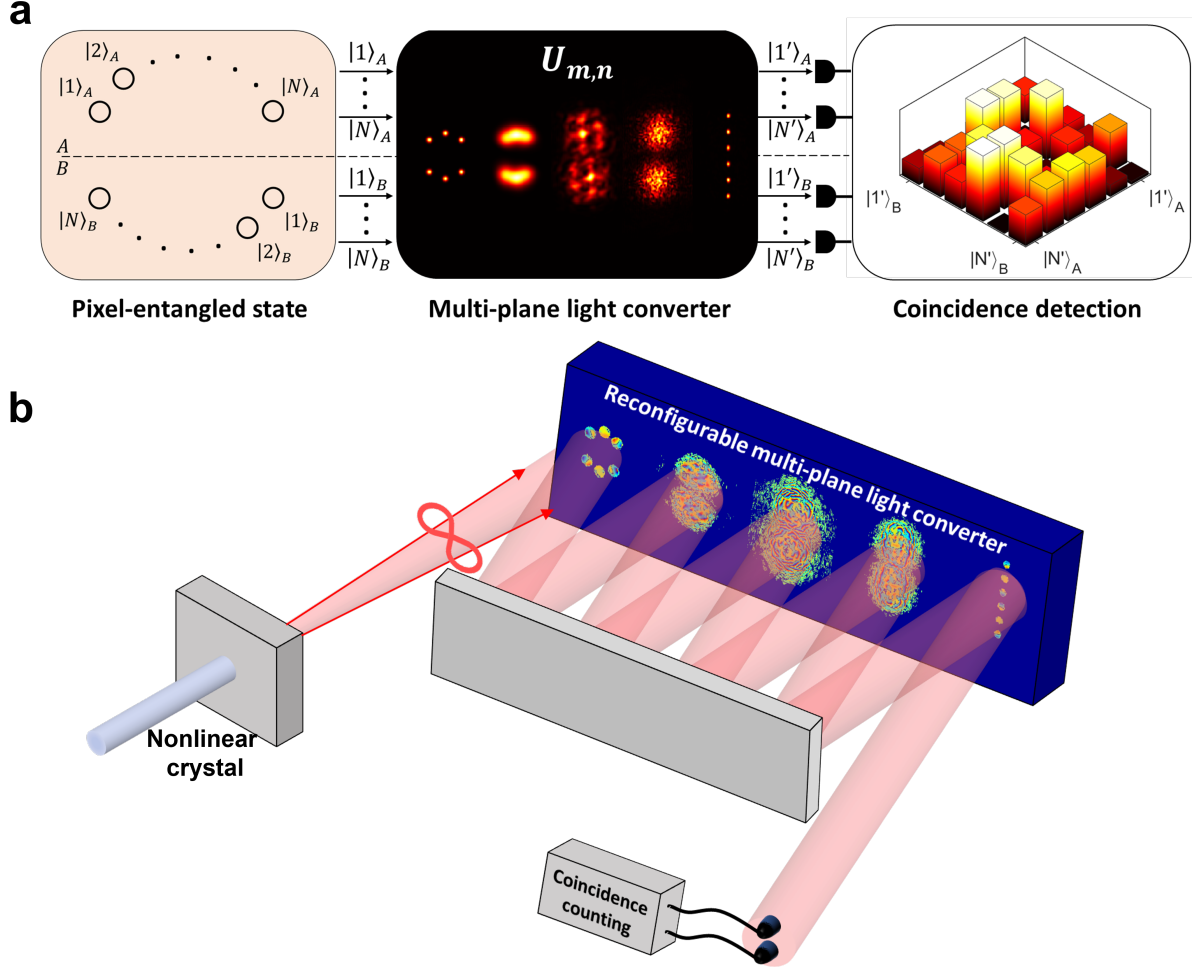


Figure 1: Reconfigurable transformation of entangled photons. (a) A pixel-entangled two-photon state, $|\psi\rangle = \frac{1}{\sqrt{N}}(|1\rangle_A|1\rangle_B + \dots + |N\rangle_A|N\rangle_B)$, undergoes a general unitary transformation implemented using a multi-plane light converter (MPLC). The output quantum correlations are measured at the last plane of the MPLC. (b) Illustration of the experimental implementation. Pixel-entangled photons are generated via spontaneous parametric down conversion. The MPLC is placed at the far-field of the nonlinear crystal and consists of five planes, implemented by successive reflection between a phase-only spatial light modulator and a mirror. The correlations between the photons are measured at the output using two scanning single photon detectors.

We begin by using the MPLC to certify high-dimensional entanglement [33, 34]. To certify entanglement in two or more dimensions, one must measure the quantum correlations between the photons in at least two MUBs [34, 41]. In our case, we utilize the reconfigurability of the MPLC to switch between measurements in the 'standard' $|1\rangle, \dots, |N\rangle$ pixel basis, and in

the discrete Fourier transform (DFT) MUB defined by $|j'\rangle_{A/B} = \frac{1}{\sqrt{N}} \sum_{m=1}^N \omega^{j(m-1)} |m\rangle_{A/B}$, where N is the dimension of the Hilbert space of each photon and $\omega = \exp(2\pi i/N)$. It was recently proved that this set of measurements is sufficient for obtaining a lower bound on the fidelity F between the inspected quantum state and a maximally entangled target state [34]. Using this bound, m -dimensional entanglement within an N -dimensional state is certified for $F > (m - 1)/N$ [34].

In two dimensions, we measure the fidelity of the state compared with the maximally entangled Bell state $|\Phi^+\rangle = \frac{1}{\sqrt{2}}(|1\rangle_A|1\rangle_B + |2\rangle_A|2\rangle_B)$. We first program the MPLC to perform the identity operation, which maps each input spot to a single output spot, without interfering them with each other. Strong correlations between the photons are obtained in this basis (fig. 2a). To get a lower bound for the fidelity, we program the MPLC to switch to the DFT basis defined above, where strong correlations are observed as well (fig. 2b). Using these two results, we certify the entanglement by obtaining a lower bound for the fidelity $F \geq 95 \pm 1\%$, significantly above the upper bound for separable states of 50% [34]. To further quantify the performance and coherence of the transformation, we look at the visibility of the quantum interference in the DFT basis, by applying a phase ϕ to one of the spots at the input plane. The quantum correlations at the output change sinusoidally with respect to this relative phase, in agreement with the theoretical prediction and with a high visibility of $94.3 \pm 0.4\%$ (fig. 2c).

In three dimensions, we perform similar measurements to obtain a lower bound for the fidelity of our state with respect to $|\psi\rangle = \frac{1}{\sqrt{3}}(|1\rangle_A|1\rangle_B + |2\rangle_A|2\rangle_B + |3\rangle_A|3\rangle_B)$. By measuring the correlations in the standard and DFT bases, we certify genuine three-dimensional entanglement by obtaining $F \geq 90 \pm 2\%$ (fig. 2d,e), which is above the upper bound of 67% obtainable with two-dimensional entanglement [33, 34]. In three dimensions, two relative phases between the different terms in the quantum state, ϕ_1, ϕ_2 , can affect the quantum interference between the photons in the DFT basis. By varying the phases of two input spots and measuring the coincidence rate between different output modes we observe quantum interference with an average visibility $93.5 \pm 0.5\%$ (fig. 2f-h), and with good agreement with the theoretical prediction (fig. 2i-k).

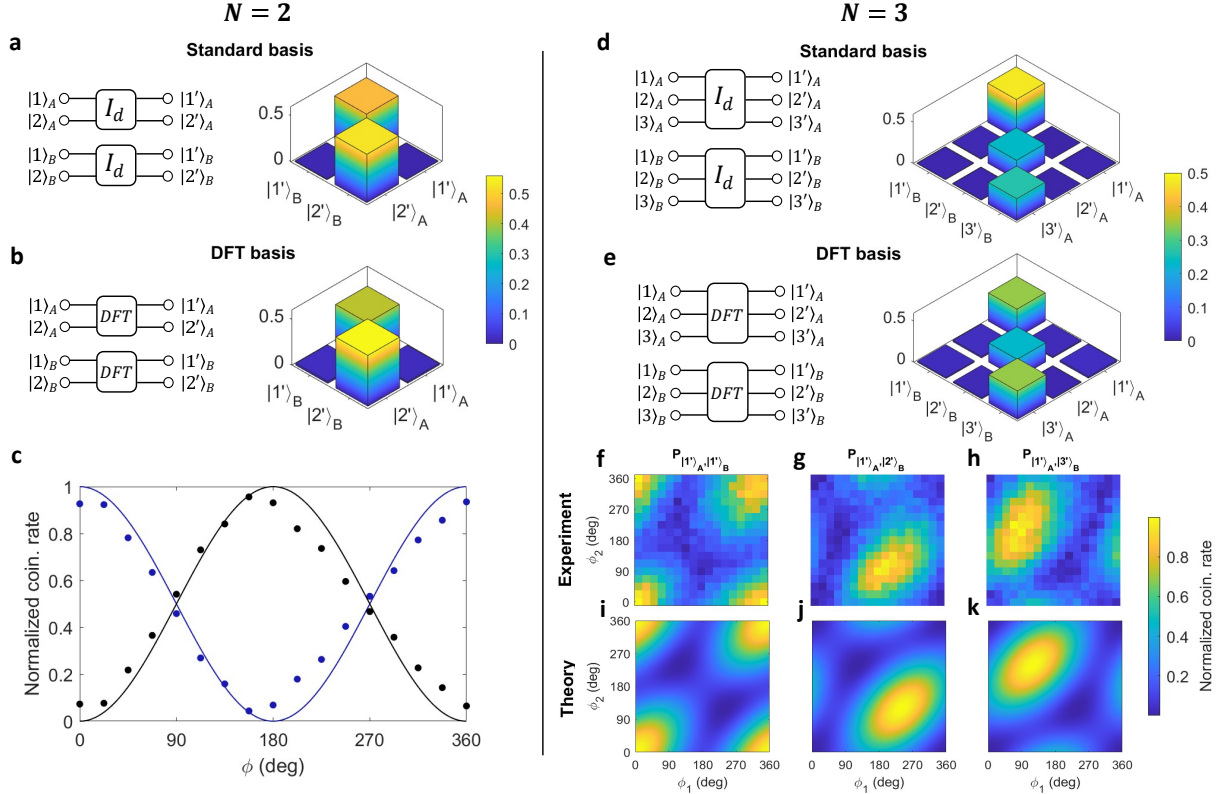


Figure 2: Entanglement certification. A maximally entangled Bell state, $|\Phi^+\rangle = \frac{1}{\sqrt{2}}(|1\rangle_A|1\rangle_B + |2\rangle_A|2\rangle_B)$, is encoded by considering the spatially entangled photons in two input spatial modes per photon, $|1\rangle_{A/B}, |2\rangle_{A/B}$. To test the fidelity of our state with respect to the maximally entangled Bell state $|\Phi^+\rangle$, measurements in the standard basis (a) and in the DFT mutually unbiased basis (MUB) (b) are performed by programming the desired transformations using the MPLC. A fidelity $F \geq 95 \pm 1\%$ is obtained, certifying entanglement. A relative phase ϕ in the input state $|\Phi^+\rangle = \frac{1}{\sqrt{2}}(|1\rangle_A|1\rangle_B + \exp(i\phi)|2\rangle_A|2\rangle_B)$ is scanned by adding the desired phase to one of the modes at the input plane of the MPLC (c). In the DFT MUB, scanning the phase ϕ switches between constructive and destructive quantum interference with high visibility, yielding the expected sinusoidal change in the coincidence rate between different modes. Next, we consider three input spatial modes per photon and measure the fidelity of our state compared with the three-dimensional entangled state $|\psi\rangle = \frac{1}{\sqrt{3}}(|1\rangle_A|1\rangle_B + |2\rangle_A|2\rangle_B + |3\rangle_A|3\rangle_B)$. Programming the MPLC to switch between the standard (d) and the DFT mutually unbiased basis (e), a fidelity $F \geq 90 \pm 2\%$ is obtained, certifying genuine three-dimensional entanglement. Similarly to the two-dimensional case, the input plane of the MPLC can be used to scan the two relative phases between the terms, ϕ_1, ϕ_2 in $|\psi\rangle = \frac{1}{\sqrt{3}}(|1\rangle_A|1\rangle_B + \exp(i\phi_1)|2\rangle_A|2\rangle_B + \exp(i\phi_2)|3\rangle_A|3\rangle_B)$. The experimental results (f-h) and theoretical predictions (i-k) for the correlations between different output modes at the MUB are in good agreement, exhibiting quantum interference with high visibility.

Next, we showcase the universality and reconfigurability of the MPLC platform by programming Haar random unitary matrices, which are of high interest for applications such as boson sampling [2, 12] and quantum cryptography [42]. We experimentally implement 400 random unitary transformations on four spatial modes, sampled according to the Haar measure [43]. For each random unitary, the coincidence rates between all pairs of output modes are measured. The probability distribution of the coincidence rates for different unitary transformations is presented in the inset of fig. 3a. For random transformations, according to the Porter-Thomas distribution, a negative exponential distribution is theoretically expected (black line) [44, 45], with good agreement with the experimental results (blue dots).

As a measure of the resemblance between the experimentally measured correlations between each pair of modes P_i^{exp} and the theoretical predictions P_i^{th} for each unitary transformation, we utilize the commonly used statistical fidelity defined as $F_s = \sum_i \sqrt{P_i^{exp} P_i^{th}}$ [2]. A histogram of the 400 statistical fidelity values is presented in fig. 3a. The average statistical fidelity obtained in our experiment is $F_s = 88.9 \pm 0.3\%$. The fidelity can be improved even further by increasing the number of planes in the MPLC. To show this, we simulate the performance of the MPLC for random transformations as a function of the number of planes (fig. 3b). Statistical fidelities of up to $98 \pm 2\%$ can be obtained by as few as 10 planes. The high statistical fidelities we obtain between the MPLC generated transformations and the target Haar transformations, manifest the capability of MPLC to generate arbitrary unitary transformations, as by definition Haar matrices uniformly sample the space of all unitary transformations [16].

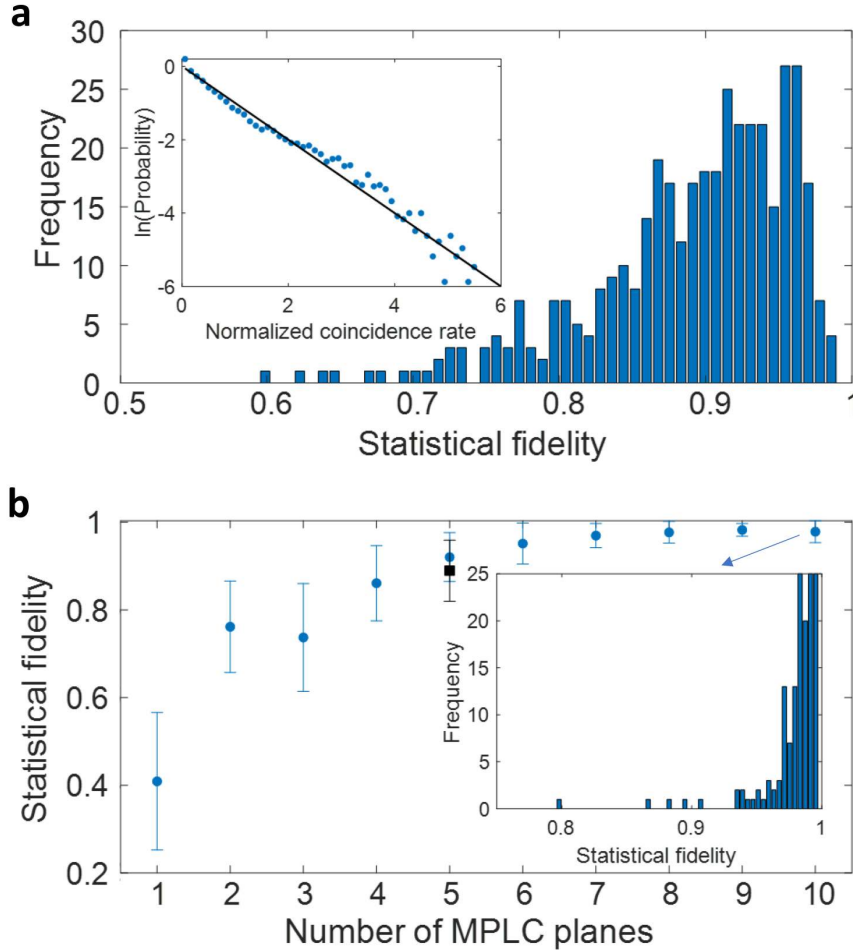


Figure 3: Programming arbitrary random transformations. We use the MPLC to experimentally implement 400 random unitary transformations on four input modes, sampled according to the Haar measure. By measuring the quantum correlations between all four output modes, the statistical fidelity compared with the theoretical prediction is calculated for each unitary. A histogram of the obtained statistical fidelities is presented in (a), showing an average statistical fidelity $F_s = 88.9 \pm 0.3\%$. In the inset, the probability distribution of the coincidence rates between the different modes normalized by their mean is presented (blue points) together with the theoretical prediction according to the Porter-Thomas distribution (black line). In (b), a simulation of the average statistical fidelity for four-mode transformations as a function of the number of planes in the MPLC is presented (blue points). Our experimental result with five planes is marked with a black square, showing good agreement with the simulated value. The histogram of the simulated statistical fidelities for an MPLC with ten planes is presented in the inset, exhibiting a statistical fidelity of $98 \pm 2\%$.

Finally, we demonstrate the relevance of MPLC for entanglement distribution [35–38]. Encoding entangled photons in modes compatible with the quantum link used for their distribution is important for reducing loss and crosstalk, making mode converters central for such applications. Here, we consider the case where Alice generates a pair of photons entangled in the pixel basis, and wishes to distribute one photon to Bob via a few-mode fiber link. Alice can thus use her MPLC to convert Bob’s photon to the LP mode basis supported by the weakly guided optical fiber, while keeping her photon in the pixel basis for ease of detection (fig. 4a). In the experiment, we consider the initial state $|\Phi^+\rangle = \frac{1}{\sqrt{2}}(|1\rangle_A|1\rangle_B + |2\rangle_A|2\rangle_B)$ generated by Alice, and program the MPLC to convert Bob’s photons such that the state $|\psi\rangle = \frac{1}{\sqrt{2}}(|1\rangle_A|LP_{01}\rangle_B + |2\rangle_A|LP_{11}\rangle_B)$ is obtained (see Methods). By keeping Alice’s detector at a fixed position and scanning the position of Bob’s detector at the output of the MPLC, we observe a correlation between the LP mode detected and the position of Alice’s stationary detector (fig. 4b,c).

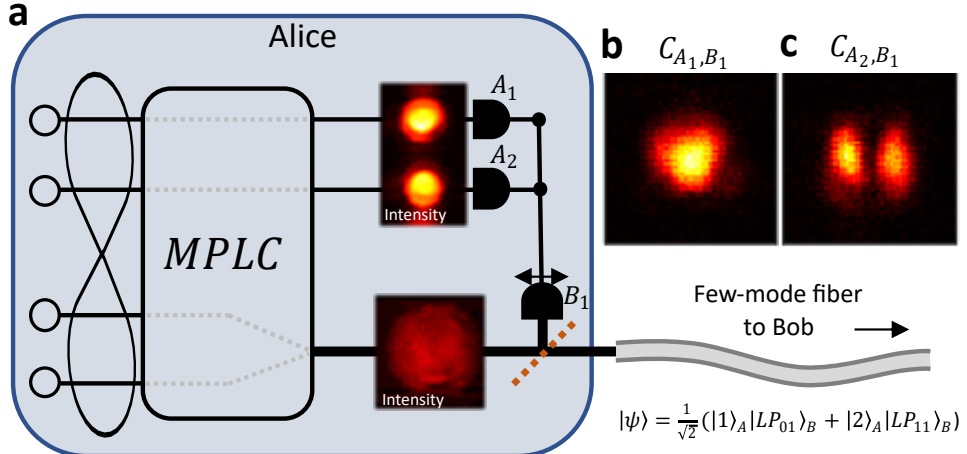


Figure 4: Mode conversion for entanglement distribution. (a) Illustration of entanglement distribution utilizing the MPLC as a mode converter. Alice generates a pixel basis entangled photon pair. The MPLC is programmed such that one of the photons is left untouched and stays with Alice, while the other is transformed from the pixel basis to a fiber mode basis and can be transmitted to Bob via a few-mode fiber link. In the experiment, we transform Bob’s photon to a LP_{01} , LP_{11} basis, and measure its spatial distribution conditioned to a detection of a photon in Alice’s top (b) or bottom (c) spots.

Discussion

In conclusion, we have demonstrated the applicability of MPLC as a building block for quantum information processing of entangled photons. We have certified high-dimensional entanglement with high fidelity by programming the MPLC to switch between different mutually unbiased bases [32, 34]. By scanning the phases of the spots at the input plane and measuring

in the DFT basis, we have observed high-visibility quantum interference, which is fundamental to many quantum information processing tasks. Furthermore, to demonstrate the universality of MPLC, we have experimentally programmed 400 Haar random unitary transformations on four modes using MPLC with five planes, observing high statistical fidelity [2]. As indicated by our simulation, near-perfect Haar random unitaries on four modes can be implemented by as few as ten planes in the MPLC. Besides demonstrating the reconfigurability and universality of the MPLC, Haar random unitaries are important for boson sampling, QKD and other quantum information processing tasks [2, 3, 12, 42]. Finally, we have considered the use of MPLC as a mode converter for entanglement distribution, demonstrating correlations between the position of one photon and the measured LP mode of the other. Being a reconfigurable, scalable and universal approach for quantum information processing that is also compatible with free-space and fiber links, MPLC can serve as a leading technology for processing high-dimensional entangled photons for quantum communication and computation. We also anticipate that the wide bandwidth of MPLC [26] together with the ability to control all degrees of freedom of light [31], will open new possibilities in controlling hyper entangled states [46].

References

- [1] O'brien, J. L., Furusawa, A. & Vučković, J. Photonic quantum technologies. *Nature Photonics* **3**, 687–695 (2009).
- [2] Carolan, J. *et al.* Universal linear optics. *Science* **349**, 711–716 (2015).
- [3] Flaminini, F., Spagnolo, N. & Sciarrino, F. Photonic quantum information processing: a review. *Reports on Progress in Physics* **82**, 016001 (2018).
- [4] Ekert, A. K. Quantum cryptography based on bell's theorem. *Physical review letters* **67**, 661 (1991).
- [5] Mayers, D. & Yao, A. Quantum cryptography with imperfect apparatus. In *Proceedings 39th Annual Symposium on Foundations of Computer Science (Cat. No. 98CB36280)*, 503–509 (IEEE, 1998).
- [6] Vazirani, U. & Vidick, T. Fully device independent quantum key distribution. *Communications of the ACM* **62**, 133–133 (2019).
- [7] Raussendorf, R. & Briegel, H. J. A one-way quantum computer. *Physical Review Letters* **86**, 5188 (2001).
- [8] Walther, P. *et al.* Experimental one-way quantum computing. *Nature* **434**, 169–176 (2005).
- [9] Giustina, M. *et al.* Significant-loophole-free test of bell's theorem with entangled photons. *Physical review letters* **115**, 250401 (2015).

- [10] Shalm, L. K. *et al.* Strong loophole-free test of local realism. *Physical review letters* **115**, 250402 (2015).
- [11] Aaronson, S. & Arkhipov, A. The computational complexity of linear optics. In *Proceedings of the forty-third annual ACM symposium on Theory of computing*, 333–342 (2011).
- [12] Zhong, H.-S. *et al.* Quantum computational advantage using photons. *Science* **370**, 1460–1463 (2020).
- [13] Matthews, J. C., Politi, A., Stefanov, A. & O'brien, J. L. Manipulation of multiphoton entanglement in waveguide quantum circuits. *Nature Photonics* **3**, 346–350 (2009).
- [14] O'brien, J. L. Optical quantum computing. *Science* **318**, 1567–1570 (2007).
- [15] Wang, J. *et al.* Multidimensional quantum entanglement with large-scale integrated optics. *Science* **360**, 285–291 (2018).
- [16] Taballione, C. *et al.* A universal fully reconfigurable 12-mode quantum photonic processor. *Materials for Quantum Technology* (2021).
- [17] Larocque, H. & Englund, D. Universal linear optics by programmable multimode interference. *arXiv preprint arXiv:2107.06107* (2021).
- [18] Van Uden, R. G. *et al.* Ultra-high-density spatial division multiplexing with a few-mode multicore fibre. *Nature Photonics* **8**, 865–870 (2014).
- [19] Sit, A. *et al.* High-dimensional intracity quantum cryptography with structured photons. *Optica* **4**, 1006–1010 (2017).
- [20] Erhard, M., Krenn, M. & Zeilinger, A. Advances in high-dimensional quantum entanglement. *Nature Reviews Physics* **2**, 365–381 (2020).
- [21] Piccardo, M. *et al.* Roadmap on multimode light shaping. *arXiv preprint arXiv:2104.03550* (2021).
- [22] Leedumrongwatthanakun, S. *et al.* Programmable linear quantum networks with a multimode fibre. *Nature Photonics* **14**, 139–142 (2020).
- [23] Matthès, M. W., del Hougne, P., de Rosny, J., Lerosey, G. & Popoff, S. M. Optical complex media as universal reconfigurable linear operators. *Optica* **6**, 465–472 (2019).
- [24] Morizur, J.-F. *et al.* Programmable unitary spatial mode manipulation. *JOSA A* **27**, 2524–2531 (2010).
- [25] Labroille, G. *et al.* Efficient and mode selective spatial mode multiplexer based on multiplane light conversion. *Optics express* **22**, 15599–15607 (2014).

- [26] Fontaine, N. K. *et al.* Ultrabroadband polarization insensitive hybrid using multiplane light conversion. In *Optical Fiber Communication Conference*, W4C–5 (Optical Society of America, 2020).
- [27] Hiekkämäki, M. & Fickler, R. High-dimensional two-photon interference effects in spatial modes. *Physical Review Letters* **126**, 123601 (2021).
- [28] Fontaine, N. K., Ryf, R., Chen, H., Neilson, D. & Carpenter, J. Design of high order mode-multiplexers using multiplane light conversion. In *2017 European Conference on Optical Communication (ECOC)*, 1–3 (IEEE, 2017).
- [29] Fontaine, N. K. *et al.* Laguerre-gaussian mode sorter. *Nature communications* **10**, 1–7 (2019).
- [30] Fontaine, N. K. *et al.* Hermite-gaussian mode multiplexer supporting 1035 modes. In *2021 Optical Fiber Communications Conference and Exhibition (OFC)*, 1–3 (IEEE, 2021).
- [31] Mounaix, M. *et al.* Time reversed optical waves by arbitrary vector spatiotemporal field generation. *Nature communications* **11**, 1–7 (2020).
- [32] Brandt, F., Hiekkämäki, M., Bouchard, F., Huber, M. & Fickler, R. High-dimensional quantum gates using full-field spatial modes of photons. *Optica* **7**, 98–107 (2020).
- [33] Friis, N., Vitagliano, G., Malik, M. & Huber, M. Entanglement certification from theory to experiment. *Nature Reviews Physics* **1**, 72–87 (2019).
- [34] Bavaresco, J. *et al.* Measurements in two bases are sufficient for certifying high-dimensional entanglement. *Nature Physics* **14**, 1032–1037 (2018).
- [35] Cirac, J. I., Zoller, P., Kimble, H. J. & Mabuchi, H. Quantum state transfer and entanglement distribution among distant nodes in a quantum network. *Physical Review Letters* **78**, 3221 (1997).
- [36] Steinlechner, F. *et al.* Distribution of high-dimensional entanglement via an intra-city free-space link. *Nature communications* **8**, 1–7 (2017).
- [37] Hu, X.-M. *et al.* Efficient distribution of high-dimensional entanglement through 11 km fiber. *Optica* **7**, 738–743 (2020).
- [38] Cao, H. *et al.* Distribution of high-dimensional orbital angular momentum entanglement over a 1 km few-mode fiber. *Optica* **7**, 232–237 (2020).
- [39] O’Sullivan-Hale, M. N., Khan, I. A., Boyd, R. W. & Howell, J. C. Pixel entanglement: experimental realization of optically entangled $d=3$ and $d=6$ qudits. *Physical review letters* **94**, 220501 (2005).

- [40] Valencia, N. H. *et al.* High-dimensional pixel entanglement: efficient generation and certification. *Quantum* **4**, 376 (2020).
- [41] Wootters, W. K. & Fields, B. D. Optimal state-determination by mutually unbiased measurements. *Annals of Physics* **191**, 363–381 (1989).
- [42] Hayden, P., Leung, D., Shor, P. W. & Winter, A. Randomizing quantum states: Constructions and applications. *Communications in Mathematical Physics* **250**, 371–391 (2004).
- [43] Zyczkowski, K. & Kus, M. Random unitary matrices. *Journal of Physics A: Mathematical and General* **27**, 4235 (1994).
- [44] Boixo, S. *et al.* Characterizing quantum supremacy in near-term devices. *Nature Physics* **14**, 595–600 (2018).
- [45] Porter, C. E. & Thomas, R. G. Fluctuations of nuclear reaction widths. *Physical Review* **104**, 483 (1956).
- [46] Deng, F.-G., Ren, B.-C. & Li, X.-H. Quantum hyperentanglement and its applications in quantum information processing. *Science bulletin* **62**, 46–68 (2017).
- [47] Agrawal, G. P. *Fiber-optic communication systems*, vol. 222 (John Wiley & Sons, 2012).

Methods

Wavefront matching. The required phase masks for every transformation presented in this work were calculated by the wavefront matching optimization method. Given a set of input and output modes defining the desired unitary transformation, an optimization process with between 20 and 50 iterations has been performed. In every iteration, each phase mask is adjusted by propagating all input modes and back-propagating the output modes to the same relevant plane, and taking their phase differences into account. Thanks to reciprocity, for a perfect transformation, the output and input modes must have the same phase profile at each plane. The algorithm thus adjust the phase at each plane so that the average error between all input and output modes is minimal (see [29] for more details and an open-access Matlab code). To avoid scattering losses and obtain smoother phase masks, we have limited the optimization algorithm to utilize angles up to only a quarter from the maximal diffraction angle determined by the pixel size of the SLM. In addition, utilizing the fact that our modes are spatially separated at the input plane, an additional phase was added to each input mode to ensure their global phases at the output are correct.

LP modes. The field distributions of the output LP_{01} and LP_{11} target modes in fig. 4 were calculated for a step index fiber with a diameter of $50\mu m$ and numerical aperture of 0.2, at the wavelength of $808nm$ [47]. The size of the actual target output modes was scaled up by a factor of ten to allow measuring them with good spatial resolution.

Data availability

The data that support the findings of this study are available from the corresponding author upon reasonable request.

Acknowledgments

Funding: This work is supported by the Zuckerman STEM Leadership Program, the Israel Science Foundation (grant No. 1268/16) and the United States-Israel Binational Science Foundation (BSF) (Grant No. 2017694). Authors contributions: O.L. and Y.B. designed the experiment. K.S. suggested useful measurements and applications. O.L. built the experimental setup, performed measurements, analyzed and interpreted the data. Y.B. supervised the project. All authors contributed to the manuscript.

Supplementary materials

Detailed experimental setup

A detailed illustration of the experimental setup is given in fig. S1. A $250mW$, $405nm$ continuous wave laser is used as a pump beam for the spontaneous parametric down conversion (SPDC) process. The pump beam is first filtered by two $40nm$ filters centered at $400nm$ to exclude any residual light at undesired wavelengths, and then focused by a $400mm$ lens onto an $8mm$ thick type-I BBO crystal, exhibiting a waist of $55\mu m$ at the crystal plane. After the crystal, a dichroic mirror is used to separate the pump beam from the entangled photons. A 2-f system with a focal length of $50mm$ followed by a 4-f system with a focal length of $150mm$ are used so that the far-field distribution of the photons is imaged onto the first plane of the MPLC.

The MPLC consists of five planes, implemented by reflecting the entangled photons between a liquid crystal SLM (pixel size $12.5\mu m$) and a dielectric mirror. Free space propagation of $76mm$ separates the different planes in the MPLC. A vertical linear phase is implemented in all areas of the SLM not used for the transformation, to allow efficient blocking of residual light by a spatial filter located after the MPLC, at the Fourier plane of the last phase mask. As the SLM modulates only horizontally polarized light, we place a polarizer at the output of the MPLC to eliminate any unmodulated light. Lenses with focal lengths $150mm$ and $250mm$ are used to image the final plane of the MPLC onto two $100\mu m$ multimode fibers connected to single photon detectors. A 50/50 beamsplitter is used to probabilistically split the light into the two detectors, which are filtered with $10nm$ filters centered around $810nm$. Coincidence counts are recorded using a dedicated FPGA, with a coincidence window of $4ns$. Accidental counts are subtracted in all coincidence measurements.

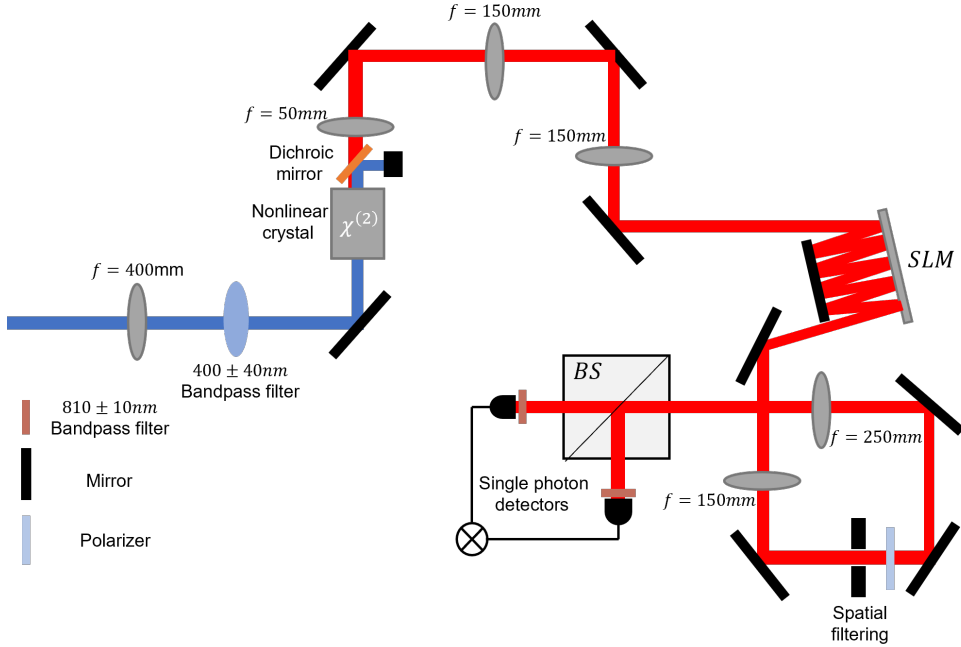


Figure S1: Detailed experimental setup.

MPLC efficiency

We define the efficiency of the MPLC as the ratio between the total intensities measured at the output and input modes of the MPLC. To estimate the efficiency of the MPLC, we consider 50 Haar random transformations on four spots (as in fig. 3), and compare for each transformation the total intensity at the relevant spots before and after the MPLC. We observe an average efficiency of $19 \pm 5\%$, which is comparable with recent demonstrations with classical light [29]. The efficiency of the MPLC in our experiment is reduced mainly due to loss (17%), the accuracy of the transformations which according to simulations reduce the efficiency by $31 \pm 8\%$, and the imperfect diffraction efficiency of the SLM. We note that in principle, MPLCs with much higher efficiencies can be achieved, using for example deformable mirrors instead of liquid-crystal SLMs.